THE UNIVERSITY of EDINBURGH

Edinburgh Research Explorer

Chemically cross-linked hydrogels from repetitive protein arrays

Citation for published version:
Boni, R, Blackburn, EA, Kleinjan, D-J, Jonaitis, M, Hewitt-Harris, F, Murdoch, M, Rosser, S, Hay, DC & Regan, L 2023, 'Chemically cross-linked hydrogels from repetitive protein arrays', *Journal of Structural Biology*, vol. 215, no. 3, 107981. https://doi.org/10.1016/j.jsb.2023.107981

Digital Object Identifier (DOI):
10.1016/j.jsb.2023.107981

Link:
Link to publication record in Edinburgh Research Explorer

Document Version:
Publisher's PDF, also known as Version of record

Published In:
Journal of Structural Biology

General rights
Copyright for the publications made accessible via the Edinburgh Research Explorer is retained by the author(s) and / or other copyright owners and it is a condition of accessing these publications that users recognise and abide by the legal requirements associated with these rights.

Take down policy
The University of Edinburgh has made every reasonable effort to ensure that Edinburgh Research Explorer content complies with UK legislation. If you believe that the public display of this file breaches copyright please contact openaccess@ed.ac.uk providing details, and we will remove access to the work immediately and investigate your claim.

OPEN ACCESS

Download date: 09. Jun. 2023

Journal of Structural Biology 215 (2023) 107981

Contents lists available at ScienceDirect

Journal of Structural Biology

journal homepage: www.elsevier.com/locate/yjsbi

Chemically cross-linked hydrogels from repetitive protein arrays

Rossana Boni [a], Elizabeth A. Blackburn [b,1], Dirk-Jan Kleinjan [c], Mantas Jonaitis [d], Flora Hewitt-Harris [a], Megan Murdoch [a], Susan Rosser [c], David C. Hay [d], Lynne Regan [a,*]

[a] Centre for Engineering Biology, Institute of Quantitative Biology, Biochemistry and Biotechnology, School of Biological Sciences, University of Edinburgh, Edinburgh, United Kingdom
[b] Edinburgh Protein Production Facility (EPPF), University of Edinburgh, Edinburgh, United Kingdom
[c] UK Centre for Mammalian Synthetic Biology, School of Biological Sciences, University of Edinburgh, Edinburgh, United Kingdom
[d] Centre for Regenerative Medicine, Institute for Regeneration and Repair, University of Edinburgh, Edinburgh, United Kingdom

ARTICLE INFO

Edited by Silvio C.E. Tosatto

Keywords:
Protein engineering
Repetitive sequence
Hydrogels
SpyTag SpyCatcher
Protein rheology
Tissue engineering
Biomaterials

ABSTRACT

Biomaterials for tissue regeneration must mimic the biophysical properties of the native physiological environment. A protein engineering approach allows the generation of protein hydrogels with specific and customised biophysical properties designed to suit a particular physiological environment. Herein, repetitive engineered proteins were successfully designed to form covalent molecular networks with defined physical characteristics able to sustain cell phenotype. Our hydrogel design was made possible by the incorporation of the SpyTag (ST) peptide and multiple repetitive units of the SpyCatcher (SC) protein that spontaneously formed covalent crosslinks upon mixing. Changing the ratios of the protein building blocks (ST:SC), allowed the viscoelastic properties and gelation speeds of the hydrogels to be altered and controlled. The physical properties of the hydrogels could readily be altered further to suit different environments by tuning the key features in the repetitive protein sequence. The resulting hydrogels were designed with a view to allow cell attachment and encapsulation of liver derived cells. Biocompatibility of the hydrogels was assayed using a HepG2 cell line constitutively expressing GFP. The cells remained viable and continued to express GFP whilst attached or encapsulated within the hydrogel. Our results demonstrate how this genetically encoded approach using repetitive proteins could be applied to bridge engineering biology with nanotechnology creating a level of biomaterial customisation previously inaccessible.

1. Introduction

The complex physiological environment of different biological tissues presents diverse cell types, tissue chemistry, tissue morphology, and mechanical stresses that are further altered by local pathology. This complex and dynamic environment may also alter the properties of implanted materials and affect their performance (Boni et al., 2018). As such, a “one size fits all” biomaterial is not appropriate to the diversity of biological needs, and real value rests in the customisation and tailoring of material design. Stem cell transplants have shown great promise towards improving behavioural recovery following injury and in amelioration of chronic or degenerative diseases (Rashidi et al., 2018; Grant et al., 2017). Engineering new stimuli-responsive hydrogels as stem cell carriers could increase the viability of stem cells, or the derivative somatic cell type, after implantation into damaged tissue and contribute to improve functional repair (Tang et al., 2019). The field of tissue engineering is moving towards the development of biological rather than synthetic hydrogels due to their biocompatibility and bioactivity (Boni et al., 2020). In particular, next generation protein-based hydrogels are exciting new candidates for tissue engineering applications, due to the precise control of the structure and function enabled by protein engineering (Schloss et al., 2016; Wu et al., 2018). The advantages of this engineering biology approach can be summarised as follows: (1) key features and requirements of the hydrogels are encoded by the protein sequence that specifies the structure; (2) virtually any desired sequence can be created by straightforward genetic engineering methods; (3)

Abbreviations: SC, SpyCatcher; ST, SpyTag; SAXS, Small-angle X-ray scattering; MSD, Mean Square Displacement; LVR, Linear Viscoelastic Region; AFP, Alpha-fetoprotein; ALB, Albumin.

* Corresponding author.
E-mail address: lynne.regan@ed.ac.uk (L. Regan).
[1] Current address: Invizius, BioCity ScotlandBo’Ness Rd, Newhouse, Chapelhall, Motherwell, United Kingdom.

https://doi.org/10.1016/j.jsb.2023.107981
Received 15 December 2022; Received in revised form 19 May 2023; Accepted 23 May 2023
Available online 26 May 2023
1047-8477/© 2023 The Author(s). Published by Elsevier Inc. This is an open access article under the CC BY license (http://creativecommons.org/licenses/by/4.0/).

stimuli - responsiveness can be controlled by engineering the interactions between building blocks; (4) biological function can be directly encoded in the material (Grove et al., 2012; Gao et al., 2016; Hughes et al., 2021). Protein hydrogels can be either physically entangled systems or permanently crosslinked hydrogels. In physical hydrogels, the polymer chains entangle, typically via hydrogen, ionic or hydrophobic bonds, and create transient junctions, resulting in weaker hydrogels and reversibility of the bonds. Conversely, in chemically crosslinked hydrogels the bonds are not reversible and the hydrogels normally present stronger mechanical properties. There are several methods of covalent crosslinking, such as thermal polymerisation and enzymatic crosslinking (Stojkov et al., 2021). Our approach is based on the design and expression of repetitive proteins programmed to form permanent covalent molecular networks. To this end, we made use of SpyTag-SpyCatcher, a pair of reactive protein partners that form a specific covalent bond between Asp-117 of SpyTag and Lys-31 of SpyCatcher (Zakeri et al., 2012). SpyTag-SpyCatcher has been shown to allow the formation of covalent molecular networks with the encapsulation of stem cells without loss of viability (Sun et al., 2014). The genetically encodable attachment of SpyTag and SpyCatcher to proteins of choice makes this an efficient approach to incorporate repetitive proteins in the hydrogel, inducing different biophysical characteristics. Here we illustrate how SpyTag and SpyCatcher can be used to create functional protein hydrogels, how the biophysical properties of the hydrogels can be fine-tuned and controlled (e.g. mechanical strength, gelling behaviour, swelling capability), and how the network is suitable for tissue engineering applications.

2. Experimental procedures

Bacterial strains, plasmids, culture conditions. The bacterial strains and plasmids used in this study are listed in the supplementary information.

Recombinant protein expression and purification. *E. coli* cells harbouring the appropriate plasmid were grown at 37 °C, 250 rpm shaking, in Luria Bertani broth to an optical density of 0.6–0.8 at 600 nm. Protein expression was induced with 1 mM IPTG and growth continued for a further 20 h at 18 °C. Cells were harvested and collected by centrifugation at 10,000 rpm for 10 min and pellets were stored at −20 °C until needed. The His-tagged proteins were purified from the frozen cells using ion metal affinity chromatography (Ni-NTA resin, Qiagen) in a batch method. Briefly, after cell disruption, whole cell lysate was incubated with 8 mL of Ni-NTA resin for an hour at 4 °C on a shaking platform. The resin was washed twice with Tris - HCl, Imidazole 20 mM buffer, pH 8 and the protein of interest was eluted using Tris - HCl, Imidazole 200 mM buffer, pH 8. Protein expression and purification were assessed by SDS-PAGE. The purified protein was then dialysed extensively against distilled water at 4 °C for 12 h, frozen at −80 °C, and then lyophilised. Lyophilised proteins were stored at −80 °C until use.

Small-angle X-ray scattering. Small angle X-ray scattering (SAXS) measurements were carried out on beamline B21 at Diamond Light Source, Didcot, UK; Experiment. no. sm32446-1; fixed camera length configuration (3.6887 m; q range 0.0045 to 0.34 $Å^{-1}$); 13.0 keV beam. 45 μL of 5 mg/mL protein was loaded onto a Superdex200 Increase 3.2/300 size-exclusion chromatography column (GE Healthcare) pre-equilibrated in 20 mM Tris, pH 8, 100 mM NaCl, 15 °C at a flow rate of 0.05 mL/min using an Agilent 1200 HPLC system. The eluting proteins were exposed to x-rays and diffraction measured on a EigerX 4 M (Dectris) detector. SAXS data reduction was performed in the Diamond Light Source software pipeline; ScÅtter (v3.1) (https://www.bioisis.net/scatter). Buffer subtraction, frame averaging, and data inspection was also carried out in ScÅtter (https://www.bioisis.net/scatter). Simple geometric parameters were calculated using ScÅtter, PRIMUS and the ATSAS 2.8.34 suite of programs (Franke et al., 2017).

Preparation of the ST:SC hydrogels. Lyophilised proteins were dissolved in distilled water at the desired concentration, at room temperature, and mixed together manually at the predetermined molar ratio. Gelation occurred spontaneously upon mixing. For urea mediated protein denaturation experiments, 1 mL of 8 M urea was added to an Eppendorf tube containing 60 μL of the hydrogel and incubated overnight. The urea-soaked hydrogels were washed with distilled water prior to further experiments.

Microrheology measurements. Polystyrene microspheres with diameter = 1 ± 0.03 μm (Polysciences, Warrington, PA) served as tracer particles. Particles were washed in ultrapure water and then diluted to give a 'bead slurry' of approximately 0.25% solids (w/v) aqueous suspension. 5 μL of SC (1 mM) were mixed with 0.5 μL of the bead slurry and pipetted onto a chambered glass slide built via double sided sticky tape (1 × 1 cm). The SC + beads mix was allowed to rest onto the glass slide for 1 min to avoid excessive drift. 5 μL of ST-SasG-ST at the predetermined molar concentration (2 mM or 4 mM) were added and mixed with the SC + beads mixture on the masked glass slide, which was subsequently sealed with a coverslip. The embedded beads were imaged at a magnification of 60x using a Nikon Eclipse Ti inverted microscope (Nikon, Japan) set up with Micromanager V1.4.19 software (Edelstein et al., 2010). The motion of approximately 50 in-frame particles was captured for a total of 6000 frames per minute using a CMOS high-speed camera (ORCA - Flash4.0 V3, Hamamatsu). The beads were imaged in real time for a minimum of 45 min and a maximum of 110 min. Particle tracking was carried out using a Python script based on the weighted centroid method (Crocker and Grier, 1996) and the ensemble-averaged mean square displacement $\langle \Delta r^2(\tau) \rangle$ was calculated. Methods were adapted from Larsen and Furst (2008).

Dynamic shear rheology. Rheological measurements were carried out using a strain-controlled TA Instruments Discovery Hybrid Rheometer (DHR-2) with a standard steel parallel plate geometry (8 mm diameter). The linear viscoelastic region (LVR) was determined via a strain sweep with strain amplitude increasing from 0.01 to 100 % and a frequency of 100 rad/s. Following each strain sweep, frequency sweeps were carried out by holding the strain at 1% and decreasing the oscillatory frequency ω from 100 to 0.1 rad/sec. The storage (G′) and loss moduli (G′′) were determined as a function of ω at 25 °C. Three independent measurements were recorded and the mean is reported.

Water content. 30 μL of ST-SasG-ST at 4 mM and 30 μL of SC at 1 mM were manually mixed together to initiate spontaneous gelation. After gelation was complete, 1 mL of ultrapure water was added to each Eppendorf tube containing the hydrogel and incubated overnight at room temperature. Excess water was removed by blotting using lint free paper and the hydrogels were weighed (W_w). Subsequently, the hydrogels were freeze-dried and weighed again (W_0). The percent water intake was calculated using: (W_w - W_0) * 100/W_0.

Cell attachment. Human HepG2-CYC1-GFP were a gift from Prof. van de Water of LACDR, Leiden University, Netherlands (Wijaya et al., 2021). The cells were maintained at 37 °C with 5% CO_2 in DMEM (Gibco) supplemented with 10% (vol/vol) FBS (Gibco), 1% L-glutamine, and 1% penicillin/streptomycin. Cells were passaged every 3 days with 0.5 mL of trypsin-EDTA (0.25%) solution (Gibco) and plated onto cell culture-treated T25 flasks. 20 μL of ST-SasG-ST and 20 μL of SC were manually mixed together to initiate gelation in a well of a 96 well plate without a poly-D-lysine coating (Greiner Bio-one, Germany) and left to gel *in situ*. The entire bottom of the well was covered by the hydrogel. The plate was seeded with HepG2-CYC1-GFP at a density of 0.01 × 10^6 cells per well and incubated at 37 °C with 5% CO_2. The medium was changed after 24 h and floating cells were removed. For counting cell numbers, the cells were detached, stained with Trypan Blue solution (0.4%, Gibco) and counted using an automated cell counter (Countess II, Thermofisher Scientific). Two tailed T tests were carried out using GraphPad Prism version 9.3.1 for Mac OS, GraphPad Software, San Diego, California USA.

Cell encapsulation. Human HepG2-CYC1-GFP cells were maintained at 37 °C with 5% CO_2 in DMEM (Gibco) supplemented with 10% (vol/vol) FBS (Gibco), 1% L-glutamine, and 1% penicillin/streptomycin.

Cells were passaged every 3 days with 0.5 mL of trypsin-EDTA (0.25%) solution (Gibco) and plated onto cell culture-treated T25 flasks. A 96 well plate without a poly-D-lysine coating (Greiner Bio-one, Germany) was seeded with HepG2 - GFP at a density of 0.01×10^6 per well. 20 μL of ST-SasG-ST at 4 mM and 20 μL of SC at 1 mM were manually mixed together with the cells to initiate gelation. We used specific molar concentrations as they allowed fast gelation of the system, needed to ensure encapsulation of the cells inside the hydrogels. The cells were incubated at 37 °C and 5% CO_2 overnight.

Fluorescence microscopy. For the cell attachment, 0.5 μL of ST-SasG-ST (4 mM) and 0.5 μL of SC (1 mM) were manually mixed together to initiate spontaneous gelation. The hydrogels were manually spotted as dots of approximately 1 μL onto a Petri dish and flooded with HepG2-CYC1-GFP cells (approximately 30,000 cells). After removal of the medium, the hydrogels were washed three times with 1 mL PBS to remove non-attached cells. Fluorescence images were obtained on a Leica DMi8 microscope equipped with a 488 nm laser for GFP excitation at magnification 4x. For the encapsulation of HepG2-CYC1-GFP, fluorescence confocal images and z-stacks were obtained on a Zeiss LSM880 microscope equipped with a 488 nm laser for GFP excitation at magnification 10x.

Protein secretion. Cell conditioned media was collected after 48 h and quantified using the commercially available ELISA kits (Alpha Diagnostic International) according to the manufacturer's instructions. AFP ELISA: 25 μL of diluted samples were added to the microwell strip plate containing immobilised AFP binding antibodies. 100 μL of Anti-AFP biotin conjugate was added to the wells and incubated for 30 min. After incubation, microwells were washed 3 times. The wells were incubated for 30 min with 100 μL anti-hAFP-HRP conjugate. This was followed up with 3 washes and 100 μL of HRP conjugate incubation for 15 min. 50 μL of stop solution was added to stop the reaction. Albumin ELISA: 100 μL of diluted samples were added to the microwell strip plate containing ALB binding antibodies and incubated for 60 min. Then, microwells were washed 4 times and 100 μL of diluted Anti-Human Albumin-HRP conjugate was added to each well and incubated for 30 min. The wells were washed 5 times. After washing, 100 μL of HRP substrate was added and incubated for 15 min. 100 μL of stop solution was added to each well to stop the reaction.

For both assays, cell-conditioned media was diluted at 1:100 in wash buffer. All the wash steps were performed using the appropriate wash buffer and all the incubation steps were carried out at room temperature. The absorbances were read at 450 nm within 30 min of stop solution addition. The mean absorbances were calculated and protein concentrations were determined using a standard curve generated from known protein standards. Data was normalised to the total cell number. Two tailed T tests were carried out using GraphPad Prism version 9.3.1 for Mac OS, GraphPad Software, San Diego, California USA.

Cell Viability. Cell viability was quantified via the commercially available MTT kit (SigmaAldrich, Germany) following the manufacturer's instructions. 20 μL of ST-SasG-ST at 4 mM were manually mixed together with 20 μL of SC3 at 1 mM or 20 μL of SC4 at 1 mM and human HepG2-CYC1-GFP were seeded in 100 μL of cell culture medium at a density of 1×10^4 per well and incubated at 37 °C with 5% CO_2 for 24 h. The next day, 10 μL of MTT labelling reagent were added to each well (final concentration 0.5 mg/ml) and incubated for four hours at 37 °C with 5% CO_2. After the incubation period, 100 μL of solubilisation solution were added to each well and incubated overnight at 37 °C with 5% CO_2. Absorbance levels were read at 570 nm using a POLARstar Omega plate reader (BMG Labtech, UK). After subtracting the background, the percentage of cell viability was calculated using the following equation: (sample absorbance/control absorbance) * 100. Two tailed T tests were carried out using GraphPad Prism version 9.3.1 for Mac OS, GraphPad Software, San Diego, California USA.

3. Results and discussion

Repetitive protein design. *S. aureus* surface protein G, SasG (PDB ID: 3TIQ), is a mechanically strong, elongated, stiff, rod-shaped protein (Gruszka et al., 2012). SasG is formed from tandem repeats of 'EG' consisting of two structurally related domains: E (50 residues) and G5 (78 residues), formed from single-layer triple-stranded β-sheets. It is readily possible to make proteins having different numbers of EG repeating units, and thus change the length of the protein, whilst keeping the core stiffness (Gruszka et al., 2015). In this study, we used a SasG composed of the core monomer GEG to form structurally rigid and strong hydrogels. Here, the SasG unit was engineered to carry two SpyTags (ST) motifs, one at each end of the chain (ST-SasG-ST), Fig. 1A, with the final length of the construct ~17 nm. The ST-SasG-ST construct was combined with two different constructs named SC3 and SC4 (~5 nm for each SpyCatcher unit). The repetitive constructs carry three or four respectively SpyCatcher (SC) units linked together by a flexible glycine-rich linker $(GGS)_2RS$, Fig. 1A. We predicted that the reaction between the two protein partners - SpyTag and SpyCatcher would result in complementary interchain crosslinking, culminating in a covalently crosslinked hydrogel, Fig. 1B. Therefore, we were interested to see how different ratios of ST:SC affected the viscoelastic properties of the resulting hydrogels and how these properties could be fine-tuned to achieve a higher degree of control over the hydrogel properties. All proteins were generated by expression in *E. coli* strain BL21 (DE3), purified via N terminal His tag using Ni-NTA resin, dialysed against distilled water, and lyophilised. The resulting proteins presented as white powders that were readily dissolved in water and, when mixed together at room temperature, underwent spontaneous gelation.

Behaviour of repetitive SC3 and SC4 arrays in solution. The behaviour in solution of the repetitive protein SasG has been characterised before (Gruszka et al., 2015). Here we investigated how tandem arrays of SC, generating the repetitive proteins SC3 and SC4, behave in solution. Both SC3 and SC4 migrate as single species in size exclusion chromatography. SEC MALS data confirms that the mass of the species in the peak is consistent with the expected mass of SC3 (41 kDa), and SC4 (54 kDa) respectively. To further characterise the solution behaviour of the species, we performed SEC SAXS analysis. Processing of the data confirmed that both SC3 and SC4 are monomeric species. The Kratky plot exhibits a rapid rise, followed by a plateau, and then falls slowly towards zero, Fig. 2A. This form of a Kratky plot is consistent with a species that contains rigid folded elements and flexible linkers. The P(r) plot confirms this interpretation of the data for both SC3 and SC4, Fig. 2B. In both P(r) plots, the first peak corresponds to the intra SpyCatcher unit distances. This peak has the highest probability because these distances are the same for each SC unit. The second peak corresponds to distances between two adjacent SC units. These intra and inter distances are similar for both SC3 and SC4 units, 30 Å and 60 Å respectively. Because of the inherent flexibility of the structures, the subsequent peaks become less defined. The maximum particle dimension, Dmax (120 Å for SC3 and 150 Å for SC4), indicates that both SC3 and SC4 are predominantly extended structures, with no indication of stacked association between SC units in the array. Taken together, these data are consistent with the SC array cartoon showed in Fig. 1.

Microrheology. The speed of gelation was investigated under different conditions to explore how gelation could be controlled, with a view to being able to optimise the gelation rate for 3D printing applications. It would be crucial to control how fast the hydrogels form to adapt the hydrogel design to biofabrication, for example to ascertain the appropriate extrusion speed. It was found that the speed of gelation was proportional to the concentration of the ST:SC components and that the speed of gelation could be controlled by changing the concentration of the core components. The rate of gelation was measured using microrheology, in which the thermal motion of embedded microspheres was used to quantify changes in the rheological properties throughout the liquid–solid (sol–gel) transition (Larsen and Furst, 2008). Fig. 3 shows a

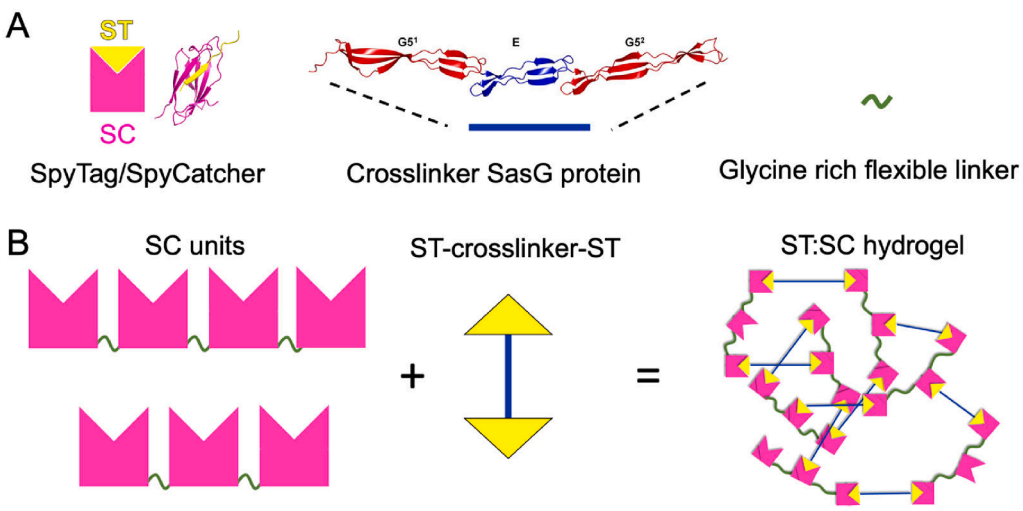

Fig. 1. Components of the SpyTag/SpyCatchers hydrogels. (A) Precursors components of the hydrogel networks. SpyTag/SpyCatcher ligase system, crosslinker SasG protein composed of the core monomer G5EG5 (PDB: 3TIQ), and the glycine rich flexible linker $(GGS)_2RS$. SpyTag in yellow, SpyCatcher in pink, SasG protein in blue, and linker in green. (B) Schematic representation of the crosslinking between the SpyTag and SpyCatchers leading to the formation of a covalently crosslinked hydrogel. Triple (SC3) and quadruple (SC4) SpyCatchers domains in pink linked together by the green glycine rich flexible linker, ST-SasG-ST crosslinker in yellow (SpyTags) and blue (SasG).

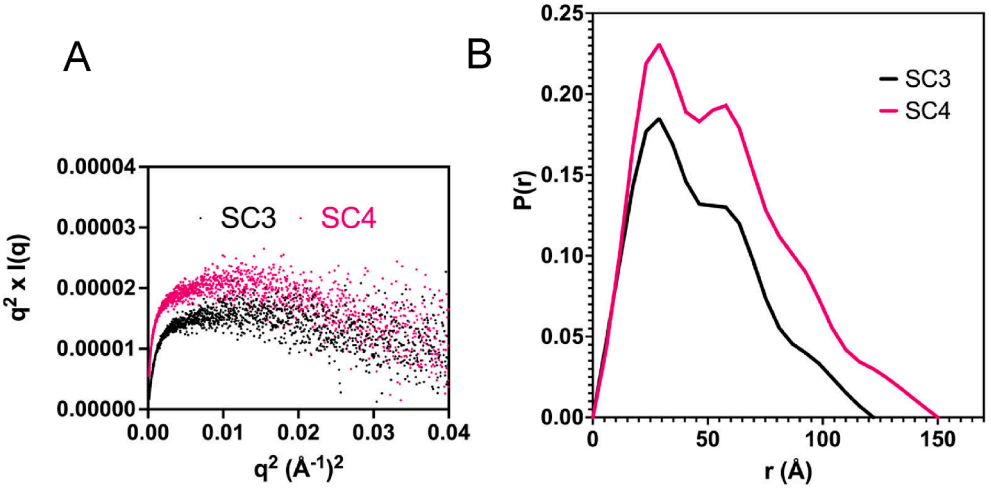

Fig. 2. SAXS studies of triple (SC3) and quadruple (SC4) linked SpyCatchers domains. SC3 in black and SC4 in pink. (A) Kratky plot of SC3 and SC4. The Kratky plot exhibits a rapid rise, followed by a plateau, and then falls slowly towards zero. This is characteristic of species that contain rigid folded elements and flexible linkers. (B) Distance distribution functions, P(r), of SC3 and SC4. The first peak (30 Å) corresponds to the intra SpyCatcher unit distances. The second peak (60 Å) corresponds to distances between two adjacent SC units. The maximum dimensions of SC3 and SC4, 120 Å and 150 Å respectively, suggest that the linked chains of SC units are predominantly in extended structures. For presentation purposes, P(r) have been scaled relative to construct length.

plot of the calculated mean square displacement (MSD) plotted against lag time (τ).

At t = 0 both systems at the two different molar ratios (SC3 = 1 mM and ST-SasG-ST = 2 mM or 4 mM respectively) showed liquid-like behaviour, characterised by free diffusion of the microparticles in the system ($\langle \Delta r^2(\tau) \rangle \approx \tau$). As the time post mixing increased, the behaviour of both systems changes. The system composed of ST:SC 2:1 mM showed a progressive and continuous decrease in the magnitude of the MSD and dependence on lag time, indicative of subdiffusive behaviour, Fig. 4A. After longer time intervals (~35–45 min) the microparticles dynamics exhibit fully subdiffusive behaviour displaying a distinct plateau and the MSD across all lag times approaches a constant value, characteristic of the formation of a viscoelastic solid. Conversely, the system composed of ST:SC 4:1mM shows a much faster decline of MSD, which approaches a constant value at ~10 min, Fig. 4B. The subdiffusive dynamics showed that the slow gelling systems are attributable to the development and growth of protein clusters in the pre-gel, culminating in the percolating network forming an infinite cluster throughout the entirety of the sample after the critical gelling point is reached. The subdiffusive dynamics were not visible in the fast-gelling system, as this combination of ST:SC reached complete gelation too quickly, indicating that the formation of an infinite protein cluster spanning the entirety of the sample was almost immediate. Combinations of ST:SC at different molar concentrations of ST (namely ST = 3 mM and ST = 3.5 mM) showed an intermediate behaviour (data not shown) where complete gelation was achieved progressively faster at ~30 and ~20 min respectively. Microrheological analysis on the system composed of ST-SasG-ST and SC4 showed a very similar behaviour, Fig. 3C and 3D. ST:SC 2:1 mM shows slows subdiffusive behaviour and progressive dependence on lag time until gelation is reached after 35–45 min. Conversely, increasing the ST content to ST:SC 4:1 mM shows a fast decline of the MSD, indicative of gelation within 10 min. Notably, comparisons between SC3 and SC4 in the slow gelling combinations shows that ST-SasG-ST combined with SC3 is marginally faster than its counterpart with SC4. This is likely due to the increased size of SC4 that leads to slower diffusivity of the protein. Due to the fast gelation kinetics of the rapidly gelling systems, differences between SC3 and SC4 are not discernible.

Thus, we showed that by subtly changing the ratio of ST:SC in the system we can control the speed of gelation of the hydrogel. Moreover, by changing the ST:SC ratios more dramatically, we were able to determine the ratios beyond which no gelation occurred (due to one of the components being present in large excess). This showed that a ratio of 2 SpyTag domains to 9 SpyCatcher domains (i.e. a ratio of 4.5:1) was incompatible with gelation. Within these established boundaries, we observed that when keeping the ST:SC ratio constant at 1:1, the rate of gelation was directly proportional to the protein concentration.

Rheology and water content. To determine the viscoelastic properties of the ST:SC hydrogels, dynamic shear rheology experiments, both strain and frequency sweeps, were carried out. Preliminary experiments determined the linear viscoelastic region (LVR) and subsequent

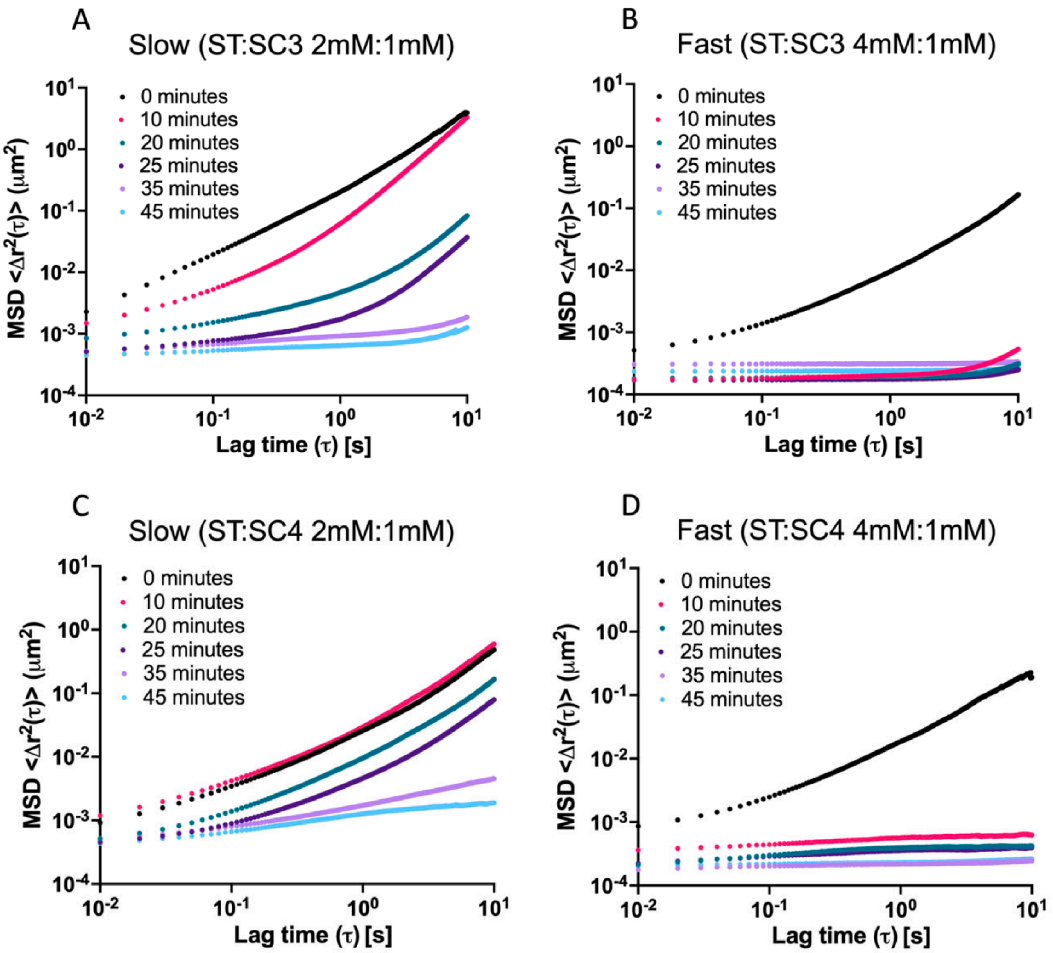

Fig. 3. Ensemble-averaged mean square displacement $< \Delta r^2(\tau) >$ of embedded polystyrene microparticles (1 ± 0.03 μm) plotted versus lag time. (A) Gelation of ST-SasG-ST at 2 mM combined with SC3 at 1 mM. (B) Gelation of ST-SasG-ST at 4 mM combined with SC3 at 1 mM. (C) Gelation of ST-SasG-ST at 2 mM combined with SC4 at 1 mM. (D) Gelation of ST-SasG-ST at 4 mM combined with SC4 at 1 mM. Individual lines represent measurements taken at different time points after mixing. The zero minute timepoint represents the data taken immediately after manual mixing of the SC and ST components to initiate gelation. The colour legend is defined in the figure. Slow gelation system gels in 35–45 min. Fast gelation system gels in less than 10 min. SC3 exhibits faster gelation kinetics compared to SC4.

frequency sweeps were conducted within the established LVR. For the network consisting of ST:SC 4 mM:1mM, the storage modulus reached a consistent value of ~1 kPa and was independent of frequency with G′>G″, indicative of typical gel like behaviour as expected for a stable, chemically crosslinked hydrogel, as shown in Fig. 4A. This network also maintained its stable storage modulus throughout the strain sweep experiment (Fig. SI1) up to 100% strain, highlighting the robustness of the network under mechanical deformation. The G′ value of this network is in good accordance with that of decellularised liver tissue, reported as 1.18 kPa (Evans et al., 2013), demonstrating the potential of the hydrogels for hepatic tissue regeneration. Conversely, in the network consisting of ST:SC 2 mM:1mM, the G′ value showed independence from frequency and G′>G″, indicative of a permanently crosslinked hydrogel. However, the G′ reached a value 10-fold higher (10 kPa) when compared to the previous network, Fig. 4B. In addition, the G′ value was maintained in the strain sweep experiment (Fig. SI1) only to 10% strain (the critical yield stress), where the gel shows a rapid decrease of the elastic modulus until G′ < G″, indicative of viscoelastic liquid behaviour. We hypothesised that this behaviour, high G′ value combined with a limited resistance to mechanical deformation, could be explained by a material that follows the behaviour given by Eq. (1) (Larson, 1999).

$$G_N^0 = \frac{\rho RT}{M_e} \quad (1)$$

where ρ is the protein density (established to be 1.35 g/cm^3 and independent from molecular weight (Matthews, 1968)), M_e is defined as the molecular weight between entanglements and G_N^0 is the entanglement plateau modulus of G′ in the appropriate frequency range (Larson, 1999). The curves presented here are all in the relevant frequency region where G′ is nearly constant, therefore G′ corresponds to G_N^0. Briefly, more crosslinks between different binding domains lead to shorter molecular weight between them, i.e a strong network, whilst fewer crosslinks translate into larger distances between them that lead to larger molecular weights and lower G_N^0. Thus, we hypothesised that the number of crosslinks is maximised in approximately equimolar ST-SC combinations, leading to lower molecular weight between crosslinks (M_e) and consequent high G_N^0 (G′ = 10 kPa). Intuitively, equimolar combinations of ST and SC yield the stiffest hydrogels, as any deviation from this ratio would lead to excess binding domains that do not contribute to the network's structure. However, the lack, or low presence, of excess binding domains could mean that the hydrogel is more brittle (critical yield stress at 10%) because when one ST crosslinker frees itself from a SC array, it will take longer for a new ST-SC connection to form given that most other crosslinkers will be already occupied, therefore the network relaxes rapidly. Conversely, when ST is present in great excess of SC, the hydrogel weakens (G′ = 1 kPa), indicating that there are fewer linkers joining up ST and SC due to the presence of dangling ends, i.e. ST attached to one end of the SC array but not linked to anything else, therefore M_e increases and G_N^0 decreases. However, the presence of dangling ends could induce the faster formation of new ST-SC crosslinks

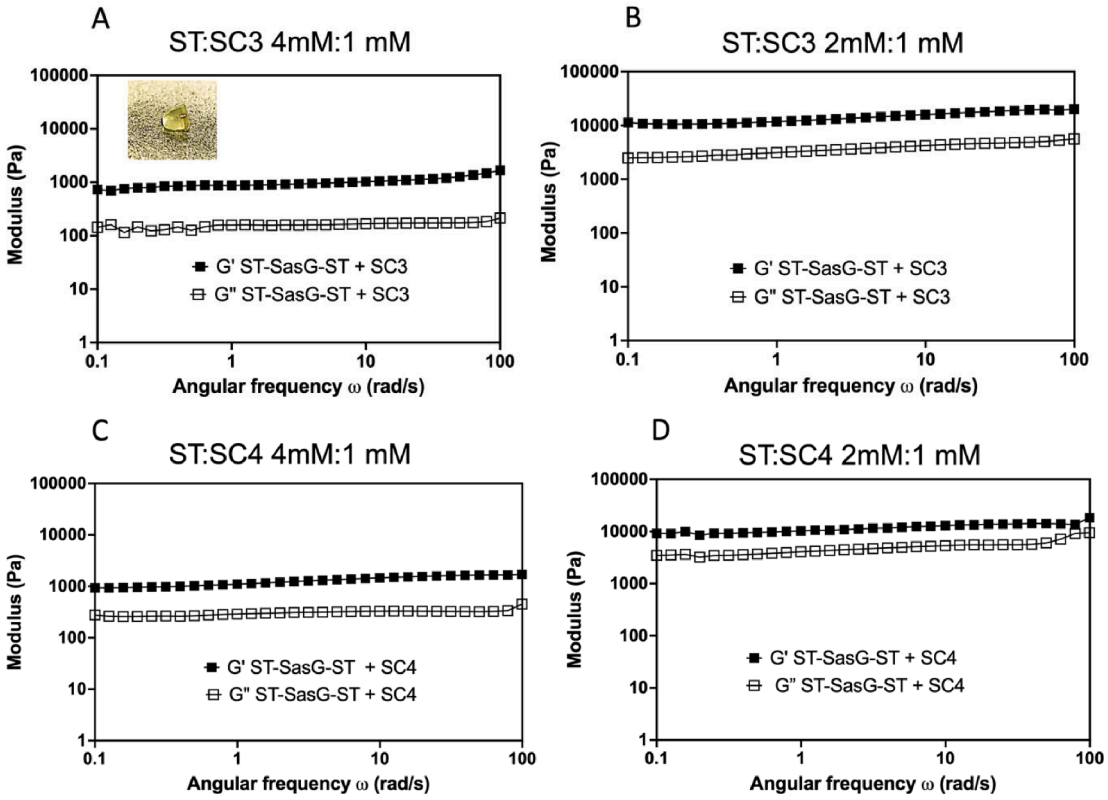

Fig. 4. The storage (G′) and loss moduli (G″) of protein hydrogels plotted as a function of angular frequency (ω). Elastic modulus (G′) in blacked boxes, loss modulus (G″) in white boxes. (A) Frequency sweep of the network consisting of ST:SC3 4 mM:1mM. G′ = 1 kPa. Insert shows a photo of a ST:SC hydrogel. (B) Frequency sweep of the network consisting of ST:SC3 2 mM:1mM. G′ = 10 kPa. (C) Frequency sweep of the network consisting of ST:SC4 4 mM:1mM. G′ = 1 kPa. (D) Frequency sweep of the network consisting of ST:SC4 2 mM:1mM. G′ = 10 kPa. G′ > G″ at low frequencies, as expected for a stable, chemically crosslinked hydrogel. Three independent measurements were recorded and the mean is reported.

once one ST-SC breaks, allowing the hydrogel to deform up until 100% strain. Interestingly, no clear differences between SC3 and SC4 can be observed in the frequency sweeps, as the two systems behave similarly. However, closer observation of the strain sweeps, Fig. SI1, shows that whilst both systems exhibit critical yield strain at ~10% strain, the reduction in G′ is faster for the SC3 system compared to SC4. This is likely due to the presence of an extra SC units in SC4 able to maintain the integrity of the hydrogel for longer before reaching the flow point (G′ < G″).

To further analyse the viscoelastic response of the hydrogels, strain and frequency sweeps were carried out on the protein hydrogels where the ST:SC ratio was kept at 1, but the absolute protein concentration was increased, see Table 1. Herein, A3 and A4 will refer to SC3 hydrogels and B3 and B4 will refer to SC4 hydrogels.

The frequency sweeps showed that below the mM concentration, (samples A1, A2, B1, B2 from Table 1), there was no hydrogel formation and the protein mixture behaved as a viscoelastic liquid (data not shown). Therefore, a minimal millimolar threshold is required to form a hydrogel using the SpyTag - SpyCatcher ligation system. We observed

Table 1
Molar concentration, ST:SC units in the SC3 or SC4 hydrogels.

SC3 [mM]	SC4 [mM]	ST-SasG-ST [mM]	N.
0.41	–	0.625	A1
0.83	–	1.25	A2
1.6	–	2.5	A3
2.5	–	3.75	A4
–	0.312	0.625	B1
–	0.625	1.25	B2
–	1.25	2.5	B3
–	1.875	3.75	B4

that the mixture A3 showed a higher modulus of ~10 kPa, Fig. SI2, but it exhibited critical yield stress at 10% strain (data not shown). Increasing the protein concentration in A4 led to a lower G′ value (~1kPa) and resistance to deformation up to 100% strain. We hypothesised that if the protein concentration in solution is increased, the crosslinking of the chains is limited by steric hinderances (Mulyasasmita et al., 2011), leading to a reduction in the hydrogel's stiffness but an increased resistance to deformation due to the presence of more unbound ST able to form a new connection with an available SC. Combinations of ST-SasG-ST and SC4 both presented G′ = 1,000 Pa and resistance to deformation up until 100% strain, Fig. SI2. Due to the increased size of SC4 compared to SC3, steric hinderances disrupting the formation of a fully percolated network are present at lower protein concentrations, leading to the differences between A3 and B3.

In addition, we tested the influence of protein folding on the hydrogel's properties. In particular, we investigated how the properties of the resulting hydrogels would change if the crosslinks remained in place but the protein building blocks were unfolded. This was performed by soaking the SC3 hydrogels in 8 M urea and carrying out strain and frequency sweeps the next day. The hypothesis was that urea treatment would unfold the protein building blocks but not influence the covalent bonds between ST and SC. Prior to the urea treatment, the hydrogels exhibited G′ = 1 kPa and no yielding up until 100% strain, Fig. 4A. As shown in Fig. SI3, after urea treatment the hydrogels still exhibited a gel-like behaviour (G′ > G″), indicative of the permeance of the ST-SC covalent bonds, unbroken by the urea denaturation. However, the hydrogel exhibited increased stiffness with G′ increased to ~10 kPa and G″ to ~5 kPa, with a consequent increase of the loss ratio δ (G″/G′), a marker of the level of unfolding in folded protein hydrogels (Hughes et al., 2022). It has been shown that a concentration of 3.2 M urea is

enough to completely unfold stable protein catenates built using the SpyTag-SpyCatcher complex (Wang and Zhang, 2016). While we did not quantify the extent of unfolding within the hydrogel, our observation on the resulting properties of the hydrogels after urea treatment suggest that significant protein unfolding occurred.

Finally, the stability and swelling properties of the gels were explored. The covalent networks were stable in excess water and they did not show any sign of erosions after 24 h in water. The water content of the hydrogels was calculated to be about ~50% after 24 h. Prior to use with cells, we tested the hydrogel stability in cell culture medium. After overnight incubation in standard DMEM cell culture medium with 10% serum (FBS), the covalent networks were stable and the gels showed no signs of degradation, confirming their suitability to cell culture and encapsulation.

Cell attachment and encapsulation. We evaluated the biological properties of the hydrogels as a suitable matrix for 3D cell culture and cell encapsulation by monitoring the growth and survival of a hepatocyte cell line, the HepG2 derived cell line HepG2-CYC1-GFP, in which a GFP reporter gene has been knocked-in into the cytochrome c1 (CYC1) gene, allowing monitoring of the cells by fluorescence (Wijaya et al., 2021). Encapsulation of the cells was achieved by adding a solution of ST-SasG-ST and SC3 together with the cells and manually mixing together the components to initiate gelation. We anticipated that the cells would prosper in the hydrogel environment due to its biological origin and suitable viscoelastic properties. After 24 h incubation in medium in the tissue culture incubator, the cells were visualised by scanning confocal microscopy. Fig. 5A shows z-stacks through the gel. We observed cells throughout the hydrogels, confirming good encapsulation. Cells presented a healthy epithelial - like morphology and expressed GFP. The straightforward encapsulation conditions contribute to make protein hydrogels a compelling choice as a platform for tissue engineering and regenerative medicine. In addition, cell attachment conditions were investigated to further evaluate the suitability of the system for tissue engineering.

We manually mixed the ST and SC components *in situ* in a 96 well plate and when gelation was complete, seeded HepG2-CYC1-GFP cells on top. After incubation for 24 h, the wells were washed to remove floating cells, and the attached cells were detached from representative wells and counted. Fresh media was then added and the cells were incubated for a further 24 h. We observed preferential cell attachment to the protein hydrogels when compared to the tissue culture plastic-only control, Fig. 5B, indicative of good biocompatibility and suitability of the hydrogels for tissue engineering applications. Imaging of the cells showed preferential cell attachment to the hydrogel and a proper level of GFP expression, suggesting good levels of cell viability, Fig. 5B. Furthermore, we assayed the conditioned media taken from the cells maintained on the 2 different hydrogels, ST-SasG-ST combined with SC3 or SC4 respectively, to determine their hepatocellular function. Using an enzyme-linked immunosorbent assay (ELISA), the amount of alpha-fetoprotein (AFP) and albumin (ALB) secreted by the cells in a 48-hour period was quantified. We observed that both alpha-fetoprotein as well as albumin secretion was similar, regardless of the hydrogel used, indicating that the cells were equally as functional on both hydrogels, Fig. 5C. Finally, we determined excellent cell viability of the protein hydrogels via an MTT assay, 91.25 ± 7.90 % cell viability for ST-SasG-ST + SC3 and 88.28 ± 5.19 % cell viability for ST-SasG-ST + SC4 (Fig. SI4), demonstrating the suitability of the protein hydrogels for tissue engineering, and specifically liver tissue regeneration.

4. Conclusions

The development of new biomaterials that can support the growth of cells for tissue regeneration is critical for their therapeutic application. In this study we showed that it is possible to make biocompatible hydrogels from flexible repetitive arrays of SpyCatcher proteins cross-linked using bi-functional SpyTag molecules in which the SpyTags are separated by stiff linkers. The resulting hydrogels support the growth and encapsulation of mammalian cells in culture. The change in properties we observed following partial denaturing of the proteins in the hydrogel using urea, supports the hypothesis that the internal structure

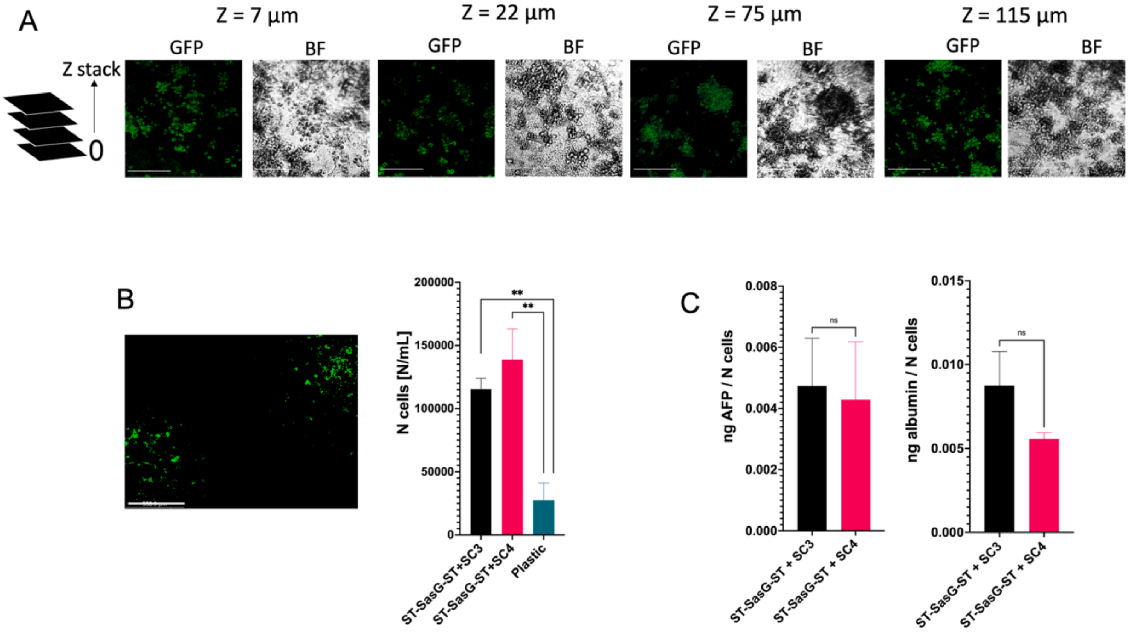

Fig. 5. ST:SC protein hydrogels are biocompatible as evaluated with the HepG2 derived cell line HepG2-CYC1-GFP. (A) corresponding BF (brightfield) and GFP Z-stacks showing cells throughout the hydrogels, confirming good encapsulation. Cells exhibit a healthy epithelial – like morphology and expressed GFP, indicative of good cell viability. Scale bars = 440 µm. (B) Quantification of cell attachment showed preferential HepG2-CYC1-GFP cell attachment to the protein hydrogels when compared to the tissue culture plastic-only control. Fluorescence imaging of HepG2-CYC1-GFP confirmed preferential cell attachment to the hydrogels and GFP expression. Scale bar = 550 µm. Data is presented as mean ± SD. (C) Quantification of alpha-fetoprotein (AFP) and albumin (ALB) secreted by the cells in a 48-hour period showed that secretion was similar on both SC3 and SC4 hydrogels, indicating that the HepG2-CYC1-GFP cells were equally as functional on both hydrogels. Data is presented as mean ± SD with N = 3 and normalised to total cell number.

of the hydrogel is dependent on the folded states of the constituent proteins and that the nature of the 'linkinG' proteins is thus essential to making a hydrogel with the desired properties. We also determined clear differences in the SC3 and SC4 hydrogels, such as the faster gelation speed of SC3 combined with ST-SasG-ST and the differences in rheological behaviour linked to the presence of an extra SC in the SC4 chain. We note that a SpyTag-SpyCatcher hydrogel that utilises a different connection between the ST units has been reported, which gives rise to very soft gels, G′ ∼ 100 Pa, (Sun et al., 2014). The hydrogels reported here present viscoelastic properties well-suited to supporting the growth of tissues of intermediate viscoelasticity, such as the liver. We have fully characterised the physical properties of our SpyTag-SasG-SpyTag + SpyCatcher protein hydrogels, both in terms of rheological and microrheological behaviour, and we showed how these properties can be fine-tuned. Our demonstration that the covalent and repetitive SpyTag-SasG-SpyTag + SpyCatcher network can support 3D cell culture and cell attachment highlights the potential of the system for tissue engineering and engineering biology.

Author Contributions.

RB, LR, and DCH led the study, designed the experiments, and wrote the manuscript with important input from EAB, MJ, and DJK. RB and MM carried out the microrheology experiments. EAB and FHH analysed and interpreted the SAXS experiments. MJ carried out the ELISA assays with guidance from DCH. RB carried out the cell culture experiments with guidance from DJK and SR. RB carried out the other experiments and data analysis. RB created the figures.

Declaration of Competing Interest

The authors declare that they have no known competing financial interests or personal relationships that could have appeared to influence the work reported in this paper.

Prof David C Hay is a founder, shareholder and director of Stimuliver ApS and Stemnovate Limited.

Data availability

All data was shared via the Excel file attached in the 'attach files' step.

Acknowledgements

RB acknowledges the support of the Medical Research Council via the Precision Medicine DTP (grant number MR/N013166/1). We also acknowledge support from the School of Biological Sciences, University of Edinburgh. Fermentations were carried out by Dr John White of the School of Chemistry Fermentation Facility at the University of Edinburgh. This work was supported by the Edinburgh Protein Production Facility (EPPF) and the Centre Core Grants (092076 and 203149) to the Wellcome Centre for Cell Biology at the University of Edinburgh. We especially thank Prof. Mark Bradley for the important discussions on rheology and for the invaluable comments on the manuscript. We also thank Dr Davide Michieletto and Dr Simon Weir for the helpful discussions on microrheology and rheology. We thank Prof. Bob van de Water for the gift of the HepG2 - CYC1 - GFP reporter cell line. We thank Dr Louise Holyoake and Fokhrul Islam for the helpful guidance and useful help during the project. Finally, we thank Dr Ella Thornton, Haresh Bhaskar, and Zoe Gidden for their comments on the manuscript and figures.

Appendix A. Supplementary material

Supplementary data to this article can be found online at https://doi.org/10.1016/j.jsb.2023.107981.

References

Boni, R., Ali, A., Shavandi, A., Clarkson, A.N., 2018. Current and novel polymeric biomaterials for neural tissue engineering. J. Biomed. Sci. 25, 90.
Boni, R., Ali, A., Giteru, S.G., Shavandi, A., Clarkson, A.N., 2020. Silk fibroin nanoscaffolds for neural tissue engineering. J. Mater. Sci.: Mater. Med. 31, 81.
Crocker, J.C., Grier, D.G., 1996. Methods of Digital Video Microscopy for Colloidal Studies. J. Colloid Interface Sci. 179, 298.
Edelstein, A., Amodaj, N., Hoover, K., Vale, R., Stuurman, N., 2010. Computer control of microscopes using μmanager. Curr. Protoc. Mol. Biol. 92.
Evans, D.W., Moran, E.C., Baptista, P.M., Soker, S., Sparks, J.L., 2013. Scale-dependent mechanical properties of native and decellularized liver tissue. Biomech. Model Mechanobiol. 12, 569–580.
Franke, D., Petoukhov, M.V., Konarev, P.V., Panjkovich, A., Tuukkanen, A., Mertens, H. D.T., et al., 2017. ATSAS 2.8: a comprehensive data analysis suite for small-angle scattering from macromolecular solutions. J. Appl. Cryst. 50, 1212–1225.
Gao, X., Fang, J., Xue, B., Fu, L., Li, H., 2016. Engineering protein hydrogels using SpyCatcher-SpyTag chemistry. Biomacromol. 17, 2812–2819.
Grant, R., Hay, D.C., Callanan, A., 2017. A drug-induced hybrid electrospun poly-caprolactone: cell-derived extracellular matrix scaffold for liver tissue engineering. Tissue Eng. Part A 23, 650–662.
Grove, T.Z., Forster, J., Pimienta, G., Dufresne, E., Regan, L., 2012. A modular approach to the design of protein-based smart gels. Biopolymers 97, 508–517.
Gruszka, D.T., Wojdyla, J.A., Bingham, R.J., Turkenburg, J.P., Manfield, I.W., Steward, A., Leech, A.P., Geoghegan, J.A., Foster, T.J., Clarke, J., Potts, J.R., 2012. Staphylococcal biofilm-forming protein has a contiguous rod-like structure. PNAS 109, E1011–E1018.
Gruszka, D.T., Whelan, F., Farrance, O.E., Fung, H.K.H., Paci, E., Jeffries, C.M., Svergun, D.I., Baldock, C., Baumann, C.G., Brockwell, D.J., Potts, J.R., Clarke, J., 2015. Cooperative folding of intrinsically disordered domains drives assembly of storng elongated protein. Nat. Comm. 6, 7271.
Hughes, M.D.G., Hanson, B.S., Cussons, S., Mahmoudi, N., Brockwell, D.J., Dougan, L., 2021. Control of nanoscale in situ protein unfolding defines network architecture and mechanics of protein hydrogels. ACS Nano 15, 11296–11308.
Hughes, M.D.G., Cussons, S., Mahmoudi, N., Brockwell, D.J., Dougan, L., 2022. Tuning protein hydrogel mechanics through modulation of nanoscale unfolding and entanglement in postgelation relaxation. ACS Nano 16, 10667–10678.
Larsen, T.H., Furst, E.M., 2008. Microrheology of the liquid-solid transition during gelation. Phys Rev Lett. 100, 146001.
Larson, R.G., 1999. The Structure and Rheology of Complex Fluids Chapter 3, 149–152.
Matthews, B.W., 1968. Solvent content of protein crystals. J. Mol. Biol. 33, 491–497.
Mulyasasmita, W., Lee, J.S., Heilshorn, S.C., 2011. Molecular-level engineering of protein physical hydrogels for predictive sol-gel phase behavior. Biomacromolecules 12, 3406–3411.
Rashidi, H., Luu, N.T., Alwashsh, S.M., Ginai, M., Alhaque, S., Dong, H., Tomaz, R.A., Vernay, B., Vigneswara, V., Hallet, J.M., Chandrashekran, A., Dhawan, A., Vallier, L., Bradley, M., Callanan, A., Forbes, S.J., Newsome, P.N., Hay, D.C., 2018. 3D human liver tissue from pluripotent stem cells displays stable phenotype in vitro and supports compromised liver function in vivo. Arch. Toxicol. 92, 3117–3129.
Schloss, A.C., Williams, D.M., Regan, L.J., 2016. Protein-based hydrogels for tissue engineering. In: Cortajarena, A., Grove, T. (Eds.), Protein-based Engineered Nanostructures. Advances in Experimental Medicine and Biology. Springer, Cham.
Stojkov, G., Niyazov, Z., Picchioni, F., Bose, R.K., 2021. Relationship between structure and rheology of hydrogels for various applications. Gels 7 (4), 255.
Sun, F., Zhang, W.B., Mahdavi, A., Arnold, F.H., Tirrell, D.A., 2014. Synthesis of bioactive protein hydrogels be genetically encoded SpyTag-SpyCatcher chemistry. PNAS 111, 11269–11274.
Tang, J.D., Mura, C., Lampe, K.J., 2019. Stimuli-responsive, pentapeptide, nanofiber hydrogel for tissue engineering. J. Am. Chem. Soc. 141, 4886–4899.
Wang, X.-W., Zhang, W.-B., 2016. Cellular synthesis of protein catenanes. Angew. Chem. 55, 3442–3446.
Wijaya, L.S., Trairatphisan, P., Gabor, A., Niemeijer, M., Keet, J., Alcalà Morera, A., Snijders, K.E., Wink, S., Yang, H., Schildknecht, S., Stevens, J., Bouwman, P., Kamp, H., Hengstler, J., Leist, M., Le Dévédec, S., Saez-Rodriguez, J., van de Water, B., 2021. Integration of temporal single cell cellular stress response activity with logic-ODE modeling reveals activation of ATF4-CHOP axis as a critical predictor of drug-induced liver injury. Biochem. Pharmacol. 190, 114591.
Wu, J., Li, P., Dong, C., Jiang, H., Xue, B., Gao, X., Qin, M., Wang, W., Chen, B., Cao, Y., 2018. Rationally designed synthetic protein hydrogels with predictable mechanical properties. Nat. Comm. 9.
Zakeri, B., Fierer, J.O., Celik, E., Chittock, E.C., Schwartz-Linek, U., Moy, V.T., Howarth, M., 2012. Peptide tag forming a rapid covalent bond to a protein, through engineering a bacterial adhesin. PNAS 109, E690–E697.